Digital Image Processing for SNDICE

E Barrelet

Laboratoire de Physique Nucléaire et de Hautes Énergies
CNRS - IN2P3 - Universités Paris VI et VII

Digital Image Processing for SNDICE

E. Barrelet

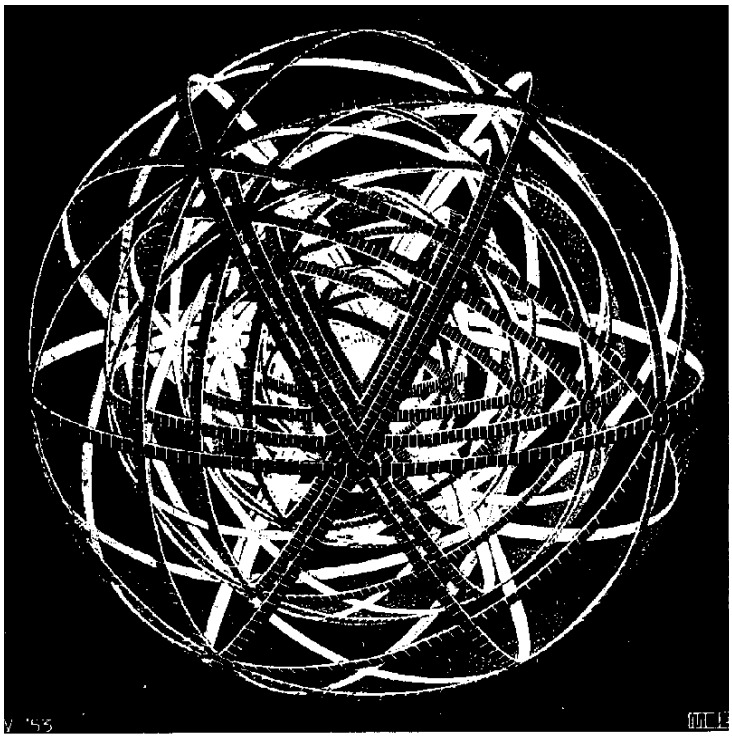

4, Place Jussieu - Tour 33 - Rez-de-Chaussée
75252 Paris Cedex 05
Tél.: 33(1) 44 27 63 13 - FAX: 33(1) 44 27 46 38

1 Introduction

We shall report here the methods developped for the analysis of diffractive ring features in Megacam images produced by SNDICE light source in a position fixed relatively to the telescope. The basic hypothesis, knowing the great stability of SNDICE illumination ($\sim 10^{-4}$), is that they are due to small angle scattering of light transmitted through the CFH telescope on small defects lying on the optical surfaces either on the primary mirror or inside the camera (including correction lens, image stabilisation unit, filter, cryostat window or CCD surface). The localization of these defects has been done in a separate report (JdBB) using a stereoscopic ray tracing method to reconstruct the position of the center of each ring system in the two images taken at two positions of the light source relative to the telescope. The point of view taken here is different. It is based on the understanding that a single image produced by Megacam record an hologram which contains all the 3-d information necessary to locate and image each defect. There is an abundant litterature concerning the application of this concept to the 3-d localization of small objects in the field of view of a digital hologram (e.g. droplets if ref??).
The three specificities of our problem reside in the system size (the huge number of pixels and of defects), in the light beam nature (not a laser) and in the variety of defect shapes.

2 Analysis methods for diffractive patterns in Megacam images

2.1 Data structure of the image and the overscan areas

A Megacam raw data image is made of 72 'amplifier blocks' numbered 0 to 71. The two amplifiers belonging to the same CCD are numbered by an even number followed by the next odd number. The CCD are numbered from 0 to 35 as shown in Figure 1, hence the amplifiers are numbered from 0 to 71 (or from 1 to 72). Each amplifier block contains 1024*4611 real pixels and a few dummy 'overscan' pixels extending the line size to 1056 pixels (electrons traversing only the full serial register) and extending the number of lines to 4644 (electrons traversing the full image area during the image readout period). The image area will be limited to 1024*4608 pixels by suppressing the last three lines, in order to exploit a 2*9 "superpixel" structure (a superpixel block is a 512*512 pixels array).
The study of Megacam-SNDICE data presented in our report LPNHE 2010-04 shows that the difference of electronic gain is the only discontinuity seen between the two parts of a CCD covered by different preamplifier. As the electronic gains are unstable at a few per mil scale, we still see a discontinuity of a few per mil at the center of the areas covered by the 36 CCDs. This problem do not affect the study of diffraction patterns across these divides. Extrapolating diffraction patterns from one CCD to the neighbour is more difficult.

2.2 Diffraction pattern detection

The aim of this section is to present some algorithms to detect the diffraction patterns seen in the SNDICE-Megacam images. We shall the reproducibility of the illumination of the focal plane, the linearity[1] of the CCD response to the sndice integrated flux and the Poisson

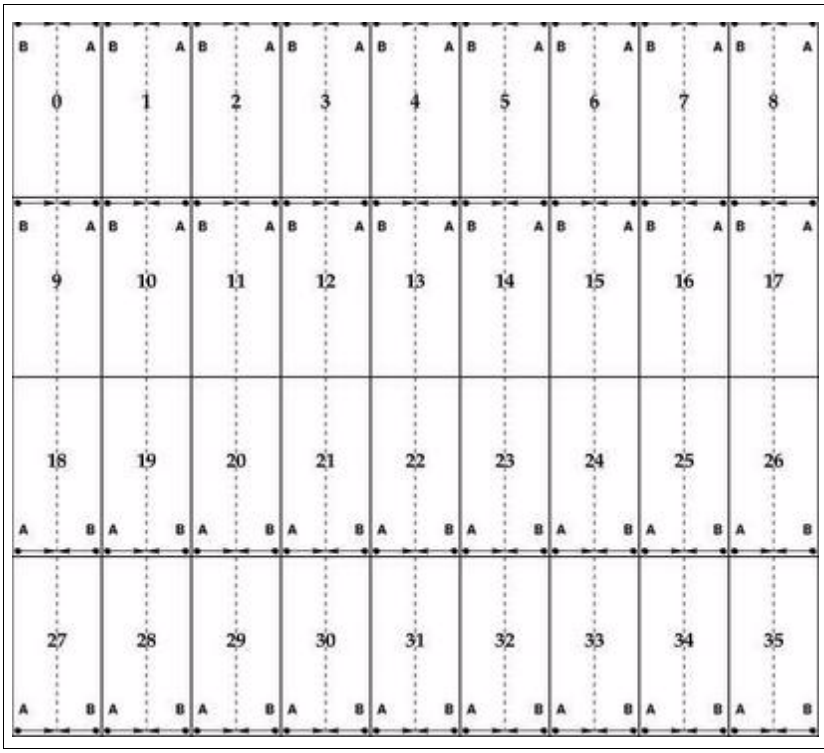

Figure 1: Megacam CCD numbering scheme (N_{CCD} =0-35). The two amplifiers A and B on each CCD are situated in a corner and the nearest pixel is read first (pixel (col=1; line=1). The amplifier number is N_{CCD}*2+0 (left amp) or N_{CCD}*2+1 (right amp).

statistical fluctuations.

Our strategy is based on detecting first the high spatial frequency patterns that are localized in the image and rarely overlap each other. We propose to filter out lower spatial frequencies using the vectorial operator of diagonal derivatives δu and δv defined by the following formulas :

$$\vec{\nabla}\Im mage\left\{pix_i^j\right\} = \begin{pmatrix}\delta u\\ \delta v\end{pmatrix} \qquad \begin{aligned}\delta u &= pix_{\ i}^{j+1} - pix_{\ i+1}^{\ j}\\ \delta v &= pix_{\ i+1}^{j+1} - pix_{\ i}^{\ j}\end{aligned} \rightarrow \begin{aligned}\rho &= \left\|\vec{\nabla}\right\| = \sqrt{\delta u^2 + \delta v^2}\\ \theta &= \arg\vec{\nabla}\end{aligned}$$

These two differential operators δu and δv are closely related to those the four spatial frequency halving operators introduced in our previous report (LPNHE 2010-04) for the analysis of Poisson noise. This is established in Appendix A

A look at the projected distributions of δu and δv (see Figure 2) shows that they are perfectly identical and symmetrical around zero. Figure 3 shows that δu and δv are not correlated. The differences Δ(δu) and Δ(δv) from one image to the next is due to the Poisson statistical fluctuations. They are superposed to δu and δv in Figure 2 and Figure 3 in order to display the signal/noise ratio. This ratio is sufficiently significant for

[1] the CCD transfer function which includes quantum efficiency, charge tranfer efficiency, preamplification, amplification and digitization is supposed identical for each pixel

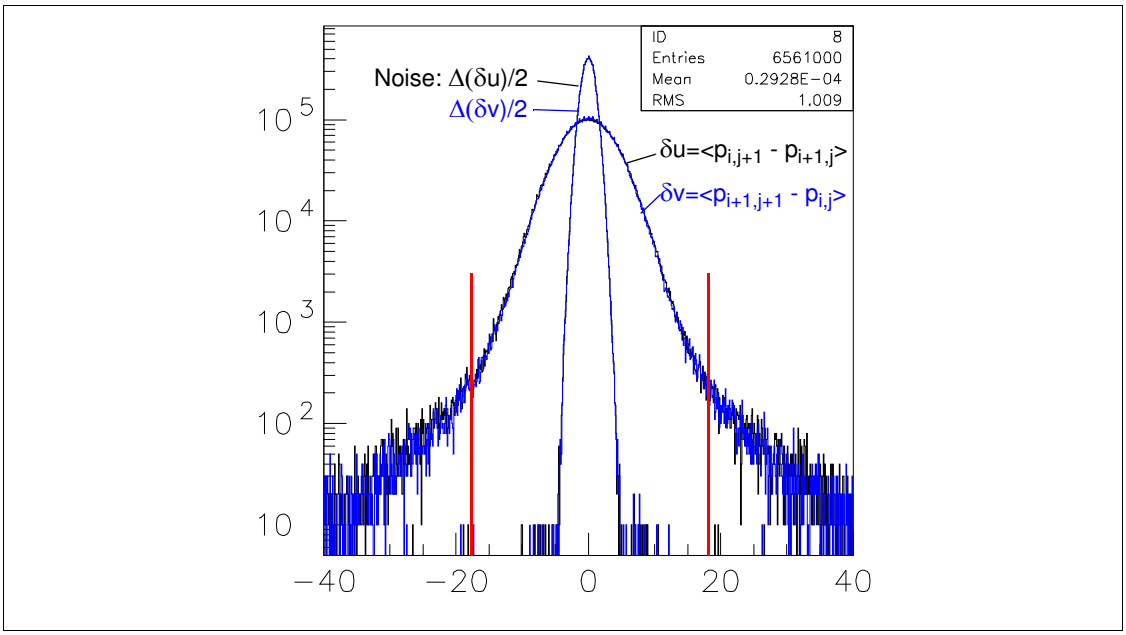

Figure 2: The distribution of the two diagonal difference operators δu and δv applied to the whole area covered by amplifier #41 are superimposed (blue and black histograms). They are normalized using the distribution of Poisson noise affecting δu and δv (gaussian law with RMS=1 centered on 0). The δu and δv estimators are computed as half sum of two consecutive images and the noise estimators are half differences of the same two images.

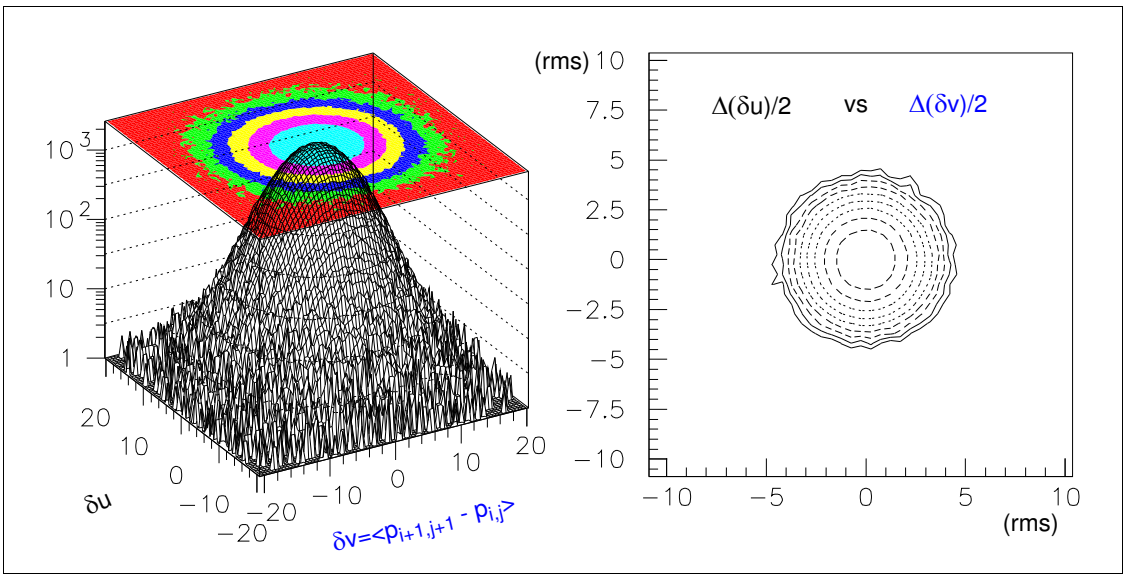

Figure 3: The frequency distribution of δu vs δv for the 4.6 millions of pixels within one amplifier (left) and the distribution of their fluctuations $\Delta(\delta u)$ vs $\Delta(\delta v)$ (right) show that they are globally uncorrelated at the scale of a full amplifier surface. This reflects the fact that diffractive ring structures have no prefered orientation at this scale. It justifies equally the use of modulus ρ and the argument θ variables to map the diffractive rings contours.

using the ρ and θ variables introduced above inside pattern recognition algorithms. Figure 4 evaluates the efficiency of a $\rho > 16\ \sigma$ cut : It selects 1% of the pixels. These selected pixels are clustered in groups such are seen in Figure 5-b) the corresponding original image in Figure 5-a). It is a rather typical case: the cluster of points is well

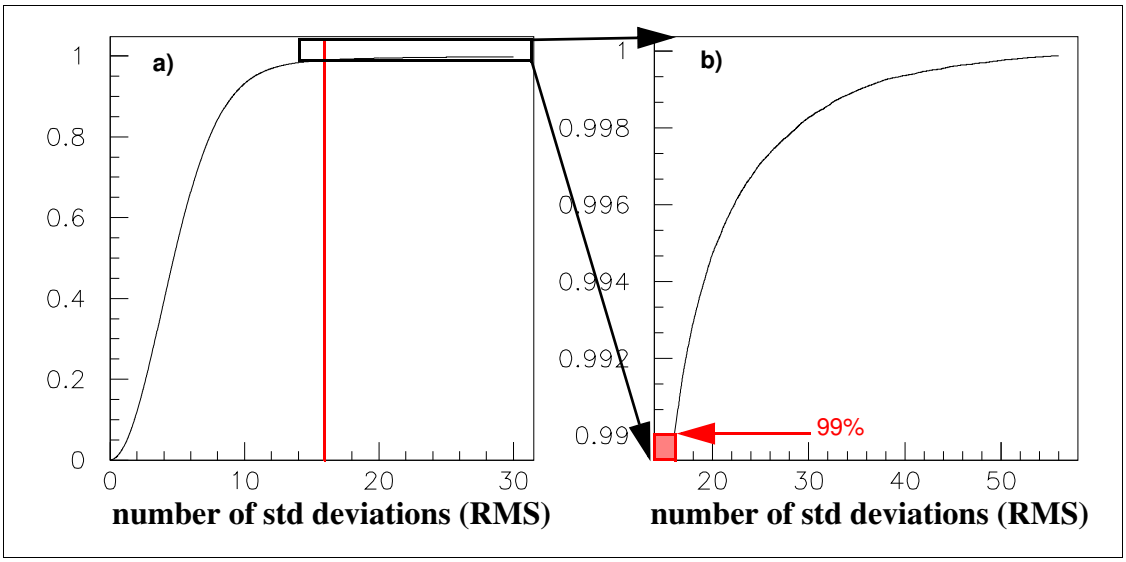

Figure 4: The cumulative distribution function of ρ =sqrt($\delta u^2+\delta v^2$) (modulus of gradient) expressed in number of standard deviation units evaluates the efficiency the cuts selecting the locations in an image where a sharp ring structure passes. For example in **a)** we mark in red a 16 σ cut which rejects 99% of the pixels. In **b)**, we zoom on the higher selectivity region. Such a 99% cut is rather practical for a pattern recognition algorithm since it produces only 46,000 points, each of them with a precision better than 7% (signal/noise) on the gradient of the local light flux distribution.

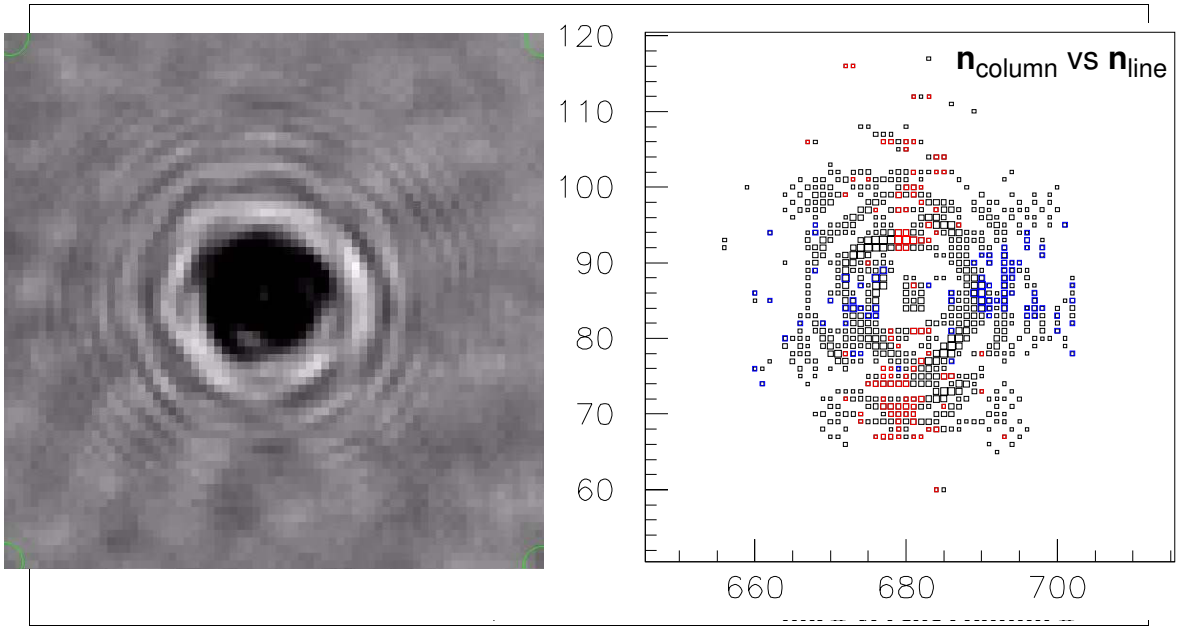

Figure 5: A small diffractive ring structure contained in a 70x70 pixel area is figured by a gray encoded image (left). The gradient of this image $\nabla = \{\delta u, \delta v\}$ is represented in a scatter plot (right) by squares proportional to its modulus $\|\nabla\|$ after the $\|\nabla\|$ >16 cut. The rejection power of this cut is represented in Figure 4. Locations where the vector ∇ is approximately horizontal (±10°) are marked in blue and vertical in red.

separated from the neighbouring ones, the circular pattern is irregular, the local orientation of the gradient visualised using a color code for the angle is correct as anticipated from Figure 3, which shows that the orientation estimator θ is not biased. This suggests that drawing contours by connecting neighbouring points of a diffraction

pattern will use not only the slope variable ρ, but also independently the orientation variable θ.
In order to see the big picture, we represent in Figure 6 the full area covered by the

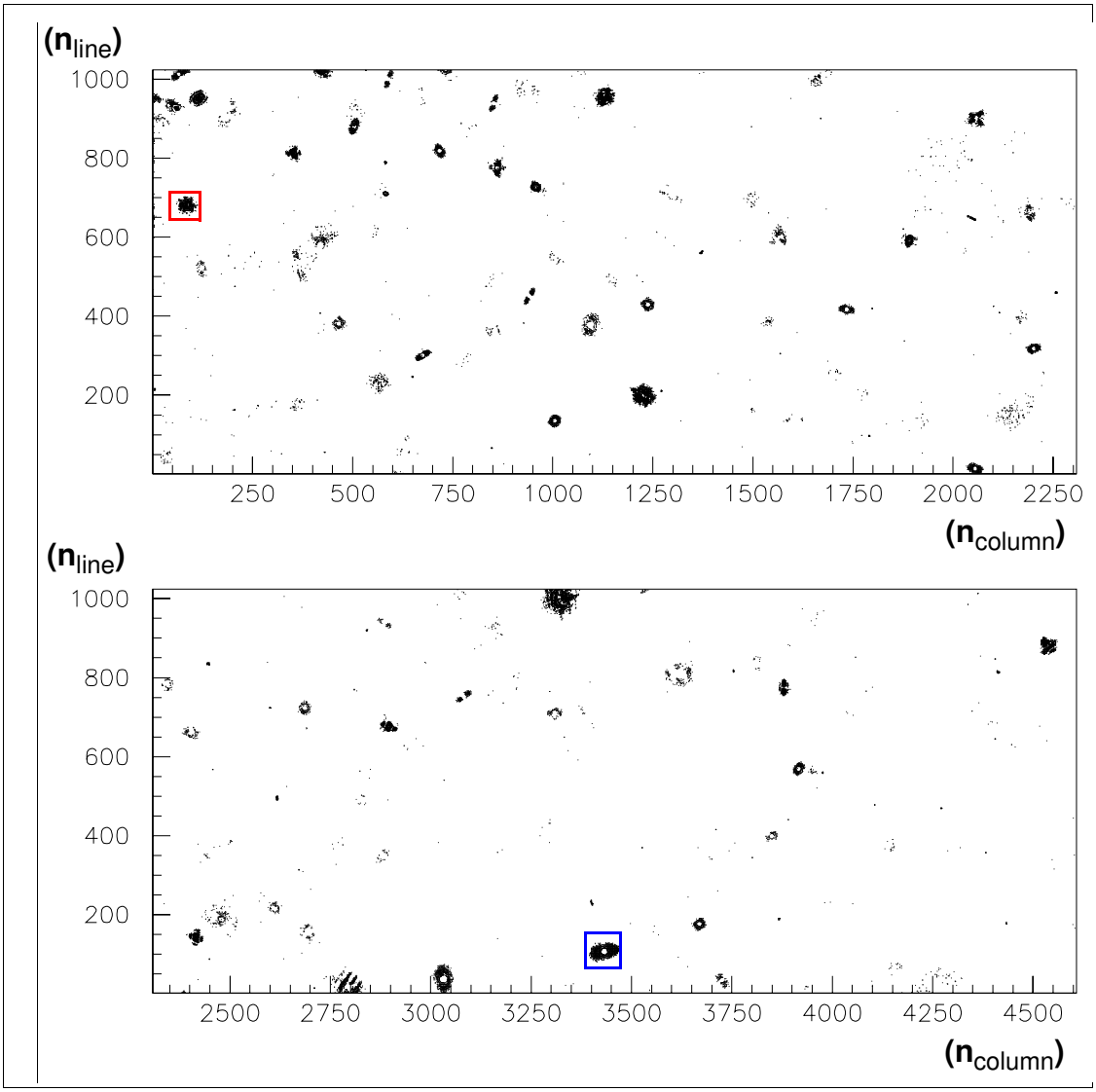

Figure 6: Megacam-SNDICE image of amplifier 40 filtered by the ρ>16 cut. The small red and blue frame frames correspond respectively to the areas enlarged in Figure 5 and Figure 7.

preamplifier 40 from which Figure 5 and Figure 7 are extracted.

2.3 Recognition of a family of concentric circles

The gradient field of a diffraction pattern with a circular symmetry is radial. This condition is usually expressed by the linearity of the slope of the field at a point belonging to a straight line as a function of the abscissa of this point.
Figure 7 illustrates this property for a diffraction pattern choosen to be circular.

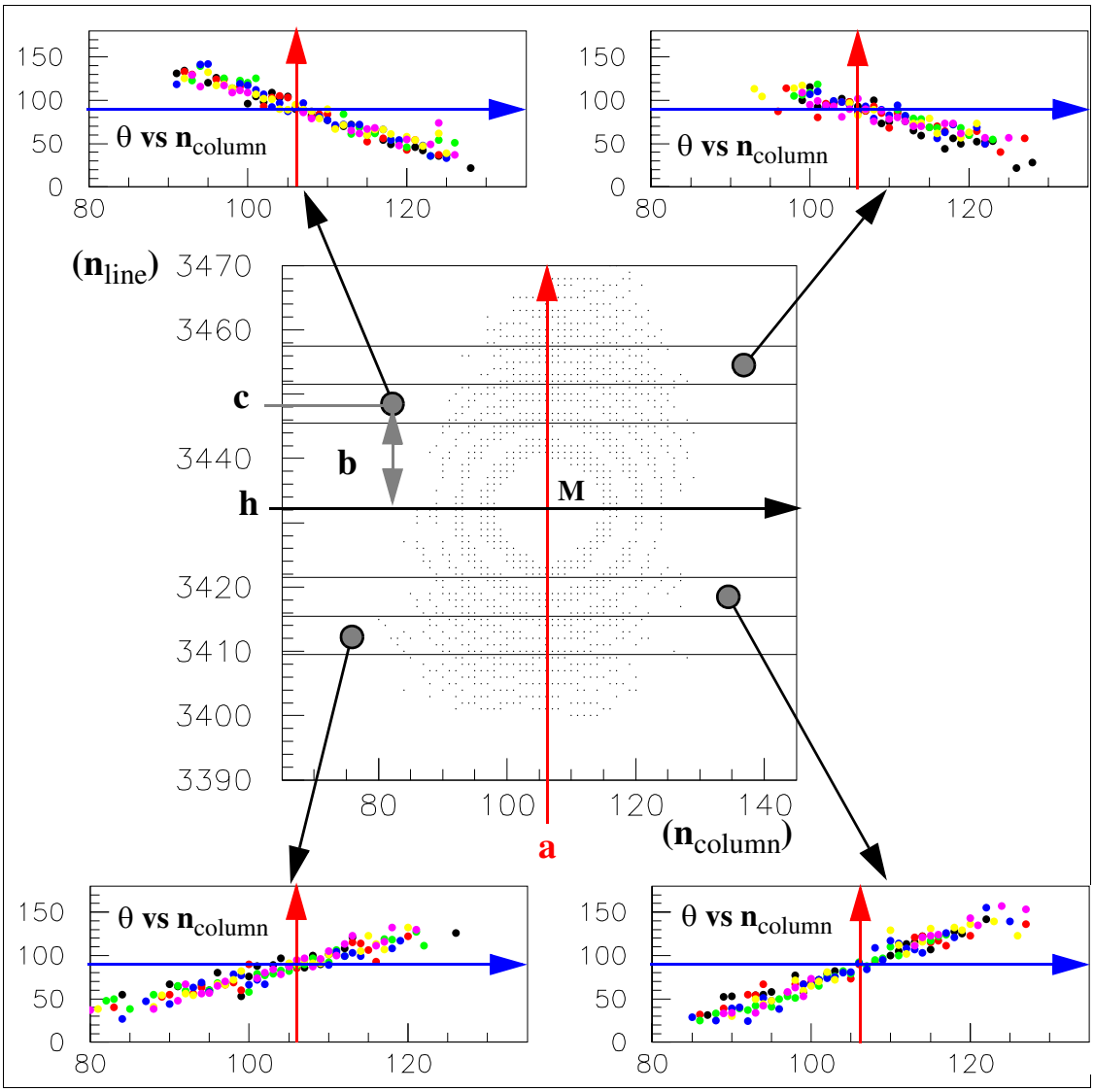

Figure 7: For a circular diffractive pattern, the y-slope of the gradient ∇ is linear in x at constant y. In this example the pattern is indicated in the central plot by the distribution of pixels where ∇ modulus is above the threshold set in Figure 4. The distribution of the argument θ as a function of the column number is given for four y slices (each made of 6 lines represented in 6 colors). One can check that for the central column x=106 (in red) the orientation of ∇ is vertical (θ=90° in blue)

The linearity condition allows to determine the center of the circular pattern by a regression analysis of slope versus position in any given line as suggested by the four scatter plots figured in Figure 7. The exact procedure consists in fitting the abscissa at origin **a** and the slope **b** and of n_{column} = **a**+ **b***cotg(θ) for n_{line}= **c** (for a band take c=<n_{line}>). The coordinates of the center **M** are (**a, h=c+b**).

The same type of analysis can be done for any particular orientation of data samples, for instance after a $\pi/2$ rotation which exchanges lines and columns. The statistical weight of a given pixel in the analysis depends on this orientation. This underlines the fact that some global bidimensional analysis[2] should be more powerful in order to exploit the

[2] a double regression in line and column indices of pixels

constraint of circular symmetry. On the contrary, for non circular diffractive patterns, one could either fraction the cluster of pixels into several approximately circular regions (‘osculating circles’) or globally estimate a central region containing the centers of curvatures of the ρ-equipotential curves.

3 Global pattern recognition strategy

3.1 Clusterisation by histogramming projections

The width of clusters obtained by applying a power threshold on a derivative image (viz. Figure 6) ranges from a few pixels to hundreds of pixels. Classically[3] histogramming the projection of a binary 2-d image on one dimension yields a fast clusterization method provided that projection of different clusters are separated. It is possible to enhance separation by selecting pixels for which the direction of the gradient vector is parallel to the projection. This reduces the lateral extension of clusters. The separation condition is fulfilled in our case provided that the image is segmented along the projection direction into ~1 Kpixels blocks. The separation of clusters projecting on the same histogram bins is obtained by rehistogramming the selected pixels along the band.

4 Appendix A

4.1 Algebra of local image processing operators

The aim of this appendix is to relate the two differential operators δu and δv introduced in previous section with the four spatial frequency halving operators introduced in our previous report (LPNHE 2010-04) for the analysis of Poisson noise.

4.1.1 recalling (Σ, Δ) operators

The (Σ, Δ) doublet creates a reversible operation yielding two images while halving the number of lines (or columns). In order to conserve an x*y symmetry we use the product $(\Sigma, \Delta)_x \times (\Sigma, \Delta)_y$. Each image yields four images with half the number of lines and half the number of columns, namely: $\Sigma_x \times \Sigma_y$; $\Delta_x \times \Sigma_y$; $\Sigma_x \times \Delta_y$; $\Delta_x \times \Delta_y$:

$\Sigma_x : (f_{i,j} , f_{i+1,j}) \rightarrow (f_{i,j} + f_{i+1,j})/2$; $\quad \Delta_x : (f_{i,j} , f_{i+1,j}) \rightarrow (f_{i,j} - f_{i+1,j})/2$
$\Sigma_y : (f_{i,j} , f_{i,j+1}) \rightarrow (f_{i,j} + f_{i,j+1})/2$; $\quad \Delta_y : (f_{i,j} , f_{i,j+1}) \rightarrow (f_{i,j} - f_{i,j+1})/2$

(The matrix element $f_{i,j}$ is the expected value of the content of the pixel in column i and line j;cf. Figure 8).

[3] pattern recognition for particle detectors

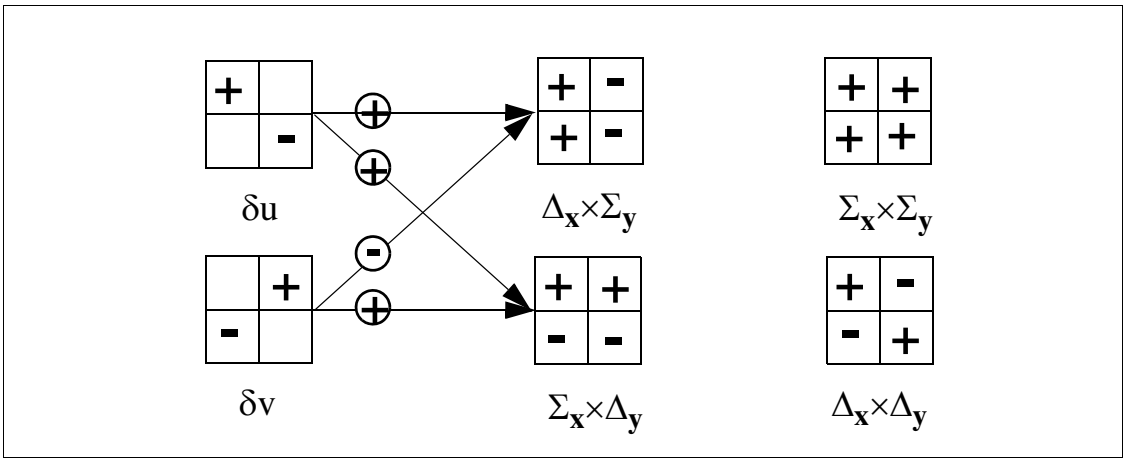

Figure 8: On the left the two diagonal derivative filters with coefficients +1/2 or -1/2. On the right the four filters acting on every pair of adjacent pixel lines (or columns) with coefficients +1/4 or -1/4 (the figure indicates the respective pattern of these coefficients and their relations)

The essential point for the analysis of photo-electron statistics is the fact that each corresponding pixels in these four images follow the same Poisson statistics. There are three images obtained with derivative operators ($\Delta_x \times \Sigma_y$; $\Sigma_x \times \Delta_y$; $\Delta_x \times \Delta_y$). Their average expected value are null. The fourth one ($\Sigma_x \times \Sigma_y$) is just the original image with a resolution reduced by a factor two.

The first two derivative operators ($\Delta_x \times \Sigma_y$; $\Sigma_x \times \Delta_y$) can be generated by the two diagonal derivative operators δu and δv introduced in previous paragraph:

$\Delta_x \times \Sigma_y = (\delta u - \delta v)/2$ and $\Sigma_x \times \Delta_y = (\delta u + \delta v)/2$

These formulas have a trivial intuitive meaning, which must be refined by taking into account the completeness issue.

The intuitive meaning of the two operators $\Delta_x \times \Sigma_y$ and $\Sigma_x \times \Delta_y$ inside the four pixel area of Figure 8 is to yield an estimate of the x and y coordinates of the gradient vector $\vec{\nabla}$. The two relations above are just expressing the effect of the 45° rotation of x,y axes into u,v axes on the coordinates of the gradient vector.

The completeness issue follows the remark that the (Σ, Δ) operator is complete. That is to say that one original megacam image yields four different sub-images, each with a number of pixel divided by four (line and column numbers are divided by 2). The process is fully reversible: no information is lost. On the contrary, if one samples δu and δv on the grid used for Σ and Δ for one every other line and one every other column, half of the information in the image corresponding to $\Sigma_x \times \Sigma_y$ and $\Delta_x \times \Delta_y$ is lost. If one samples δu and δv on the complete grid, at every line and every column as we did in 2.2, we recover all the information apart from two global constants. Taking into account the fact that the number of pixel combinations is halved but the number of samples is multiplied by four we gather that the gradient field (δu,δv) sampled on the full image grid is redundant. This type of oversampling of the image does not impede using the data for pattern recognition.